Meshless Method with reduced integration – high performance

***Wilber Vélez[1], Tiago Oliveira[1], Elvis Pereira[1] and †Artur Portela[1]**

[1,] Department of Civil and Environmental Engineering, University of Brasília, BR.

*Presenting author: wilbervelez@hotmail.com
†Corresponding author: aportela@unb.br

Abstract

The work theorem establishes an energy relationship between a statically – admissible stress field and an independent kinematically – admissible strain field in a local region. The Meshless Method with reduced integration (IMFM) is derived through a weighted-residual formulation that leads to the work theorem of structures theory.

In the formulation of the IMFM, the kinematically – admissible strain field is chosen as the one corresponding to an arbitrary rigid – body displacement; as a consequence, the domain term is canceled out and the work theorem is reduced to regular local boundary terms only. The Moving Least Squares (MLS) approximation of the elastic field is used to construct the trial function in this local meshless formulation. IMFM has a highly performance in problems with irregular nodal arrangement leading to accurate numerical results in two-dimensional elasticity problems.

This paper presents the size effect of the irregularity nodal arrangement (c_n) on energy and displacement relative error to solve the Timoshenko cantilever beam using different parameters of the local support domain (α_s), the local quadrature domain (α_q) and three different nodal discretization. Results are compared with the exact solution and the Meshless Local Petrov–Galerkin (MLPG) method and optimal results have been obtained for 2D problems plane stress.

Keywords: Meshless Method with reduce integration (IMFM), Meshless Local Petrov-Galerkin (MLPG), work theorem, Moving Least Squares (MLS), irregular nodal arrangement.

Introduction

Numerical methods based in grid, like Finite Element Method (FEM), are widely used for scientific researches. Grid-based methods required high quality meshes to solve fracture mechanics problems with material discontinuity, large deformation where excessive mesh distortion takes place and other situations. The meshless methods were generated with the expectation of providing more adaptive, accurate and stable numerical solutions that can deal with problems where conventional methods are not suitable [1]. Generally, their formulation is based in the weighted-residual method [2].

Different meshless methods have been developed during the last 20 years [3]. Some methods based on a weighted-residual weak-form formulation were applied in solid mechanics such as the Diffuse Element Method (DEM) [4], the Reproducing Kernel Particle Method (RKPM) [5], and the Element-free Galerkin (EFG) [6], were the first. After, other methods emerged based on local weighted-residual weak forms, such as the Meshless Local Petrov-Galerkin Method (MLPG) [7,8], the Meshless Local Boundary Integral Equation (MLBIE) [9], the Local Point Interpolation Method (LPIM) [10], Local Radial Point Interpolation Method

(LRPIM) [11], the meshless Finite Volume Method (FVM) [12], the Rigid-Body Displacement Mesh-Free (RBDMF) and the Generalized-Strain Mesh-Free (GSMF) [13].

The Meshless Method with reduce integration (IMFM) formulation presented by [14], the kinematically – admissible strain field is chosen as the one corresponding to an arbitrary rigid – body displacement; as a consequence, the domain term is canceled out and the work theorem is reduced to regular local boundary terms only. The Moving Least Squares (MLS) approximation of the elastic field is used to construct the trial function in this local meshless formulation. IMFM and the popular MLPG using the MLS approximation, this fact allowing to have more precise conclusions when comparing the two methods.

This paper is focused on the size effect of the configuration parameters of the local support domain (α_s), the local quadrature domain (α_q) and irregularity nodal arrangement (c_n). It presents a comparison of the energy and displacement relative error for three different irregular nodal distribution to solve the Timoshenko cantilever beam. The results are compared with the exact solution and the Meshless Local Petrov–Galerkin (MLPG) method, optimal parameters have been determined.

Methodology

Let Ω be the domain of a body and Γ its boundary subdivided in Γ_u and Γ_t that is $\Gamma = \Gamma_t \cup \Gamma_u$, as represented in Fig. 1. The general fundamental boundary value problem of linear elastostatics aims to determine the distribution of stresses $\boldsymbol{\sigma}$, strains $\boldsymbol{\varepsilon}$ and displacements $\mathbf{u}$, throughout the body, when it has constrained displacements $\bar{\mathbf{u}}$, on Γ_u and is loaded by an external system of distributed surface and body forces with densities denoted, respectively by $\bar{\mathbf{t}}$, on Γ_t and $\mathbf{b}$, in Ω.

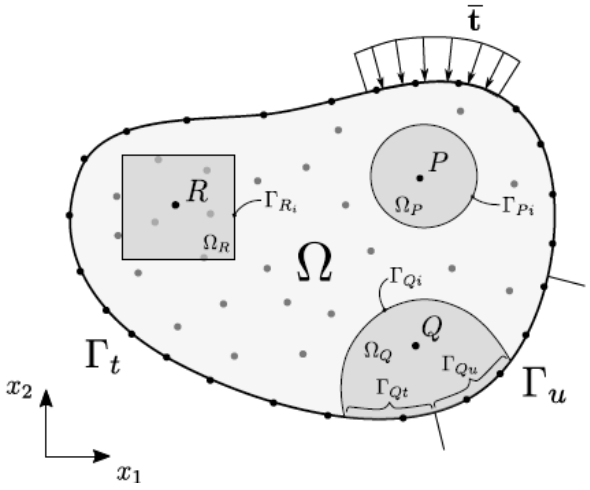

Figure 1. Meshless discretization of the global domain Ω and the local domains Ω_P, Ω_Q and Ω_R, with boundary $\Gamma = \Gamma_u \cup \Gamma_t$ represented.

The solution of these problem is a totally admissible elastic field that simultaneously satisfies the kinematic admissibility and the static admissibility. If this solution exists, it can be shown that it is unique, provided linearity and stability of the material are admitted [15, 16].

In the domain of the body, loaded by a system of external distributed surface and body forces with densities denoted, respectively by $\bar{\mathbf{t}}$, on the boundary Γ_t and $\mathbf{b}$, in the domain Ω, consider a statically admissible stress field $\boldsymbol{\sigma}$, that is any stress field that satisfies equilibrium with the system of applied external forces which therefore satisfies

$$\mathbf{L}^T\boldsymbol{\sigma}+\mathbf{b}=0 \tag{1}$$

in the domain Ω, with boundary conditions

$$\mathbf{t}=\mathbf{n}\boldsymbol{\sigma}=\bar{\mathbf{t}}, \tag{2}$$

on the static boundary Γ_t, in which $\boldsymbol{\sigma}$: Stress components, **L**: Matrix differential operator, **t**: represents the traction components, $\bar{\mathbf{t}}$: Prescribed tractions values, **n**: Unit normal components to the boundary.

In the domain Ω, with boundary $\Gamma = \Gamma_t \cup \Gamma_u$, consider an arbitrary local domain Ω_Q, assigned to a reference point $Q \in \Omega_Q$, with local boundary $\Gamma_Q = \Gamma_{Qi} \cup \Gamma_{Qt} \cup \Gamma_{Qu}$, in which Γ_{Qi} is the interior local boundary, while Γ_{Qt} and Γ_{Qu} are local boundaries that share the global boundaries, respectively the static boundary Γ_t and the kinematic boundary Γ_u, as represented in Fig. 1. The work theorem is derived as a local form that is valid in an arbitrary domain Ω_Q, associated to the reference point Q.

The general work theorem of the theory of structures stablishes an energy relationship, valid in an arbitrary local domain $\Omega_Q \cup \Gamma_Q \in \Omega \cup \Gamma$, between two independent elastic fields that can be defined in the body which are, respectively a statically admissible stress field that satisfies equilibrium with a system of external distributed surface and body forces, and a kinematically admissible strain field that satisfies compatibility with a set of constrained displacements. Derived as a weighted residual statement, the work theorem serves as a unifying basis for the formulation of numerical models Continuum Mechanics [17].

Expressed as an integral local form, defined in the local domain $\Omega_Q \cup \Gamma_Q$, which can be written in a compact form as

$$\int_{\Gamma_Q} \mathbf{t}^T\mathbf{u}^* d\Gamma + \int_{\Omega_Q} \mathbf{b}^T\mathbf{u}^* d\Omega = \int_{\Omega_Q} \boldsymbol{\sigma}^T\varepsilon^* d\Omega \tag{3}$$

in which the stress field $\boldsymbol{\sigma}$ and the strain field $\boldsymbol{\varepsilon}^*$ are not linked by any constitutive relationship and therefore, they ae independent of each other.

Kinematic formulations consider, in the work theorem, a particular and convenient specification of the kinematically admissible strain field, leading thus to an equation of mechanical equilibrium that is used in numerical models, to generate the respective stiffness matrix of each model. A simple case of local equilibrium equations, based on a kinematically admissible strain field generated by a rigid-body displacement.

Bearing in mind the key feature of the work theorem, which is the complete independence of the statically admissible stress field $\boldsymbol{\sigma}$ and the kinematically admissible strain field $\boldsymbol{\varepsilon}^*$, the strain field can be conveniently defined by a rigid-body displacement that is

$$\mathbf{u}^*(\mathrm{x})=\mathbf{c}, \tag{4}$$

where **c** is a constant vector that conveniently leads to null strains that is

$$\varepsilon^*(\mathrm{x})=\mathbf{0}. \tag{5}$$

When considered the kinematecally admissible strain field generated by arbitrary rigid-body displacement, Eq. (4), the local form of the work theorem, Eq. (3), leads to the next expression

$$\int_{\Gamma_Q - \Gamma_{Qt}} \mathbf{t}\, d\Gamma + \int_{\Gamma_{Qt}} \bar{\mathbf{t}}\, d\Gamma + \int_{\Omega_Q} \mathbf{b}\, d\Omega = 0 \tag{6}$$

which states an integral form of mechanical equilibrium, of tractions and body forces, in the local domain $\Omega_Q \cup \Gamma_Q$, are represented in Fig. 2.

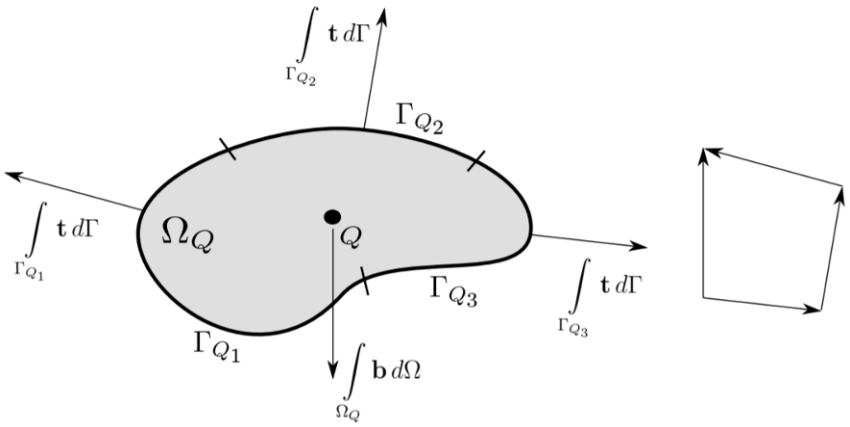

Figure 2. Schematic representation of the equilibrium of tractions and body forces, pointwisely defined at collocation points of a local form of the work theorem associated with a field node *Q*.

The modelling strategy adopted in this paper, is based in the application of the work theorem, in the set of kinematically admissible strain fields, to solve the actual elastic problem. Consider the local form of the work theorem, Eq. (3). To derive the equilibrium equations of the numerical model, the kinematic formulation of the local form is carried out through the specification of an appropriate kinematically admissible strain field $\boldsymbol{\varepsilon}^*$. This paper considers the arbitrary rigid-body displacement formulation that leads to the local form of equilibrium Eq. (6), in which are then used to generate the stiffness matrix of the meshfree numerical model.

The statically admissible stress field σ, which is required to satisfy equilibrium with a system of external forces, is assumed as the stress field that settles in the body, when it is loaded by the actual system of external distributed surface and body forces, with the actual displacement constraints.

Recall that the elastic field that settles in the body is the only totally admissible elastic field that satisfies the given problem. Therefore, besides satisfying static admissibility, through Eq. (1) and (2), that is the same as satisfying equilibrium through Eq. (6), generated by the weak form Eq. (3) of the work theorem, this unique totally admissible elastic field also satisfies kinematic admissibility defined as

$$\boldsymbol{\varepsilon} = \mathbf{L}\mathbf{u}, \tag{7}$$

in the Defining the Statically Admissible Stress Field domain Ω, with boundary conditions

$$\mathbf{u} = \bar{\mathbf{u}}, \tag{8}$$

on the kinematic boundary Γ_u, in which the displacement u is assumed continuous with small derivatives, to allow for geometrical linearity of the strain field $\boldsymbol{\varepsilon}$. Hence, Eq. (8), which specifies the constraints of the actual unique solution of the elastic problem must be fulfilled.

For the sake of simplicity, this paper considers the formulation of the meshfree numerical methods in the absence of body forces. Consequently, the equations of equilibrium are always defined only on the boundary of the local domain.

The essential feature of meshfree numerical methods is that they perform the discretization of the problem domain and boundaries with a set of scattered field nodes that do not require any mesh for the approximation of the field variables. The meshfree method IMFM, presented in this paper, is based on the moving least-squares (MLS) approximation, introduced by [18].

The MLS approximation is considered to be one of the best methods to approximate data with a good accuracy. Circular or rectangular local supports centered at each nodal point can be used. In the region of a sampling point X, the domain of definition of MLS approximation is the subdomain Ωx, where the approximation is defined, as showed in the Fig. 3

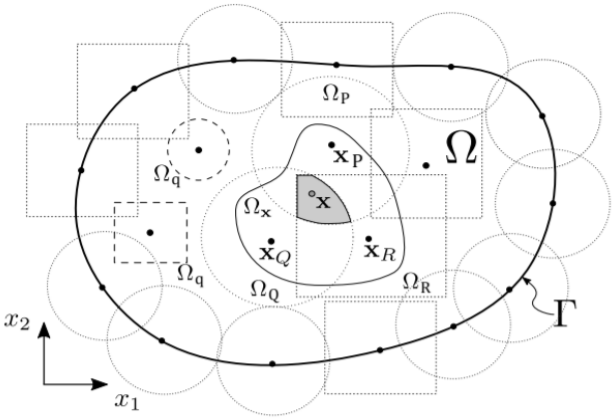

Figure 3. Representation of a global domain Ω and boundary Γ in the meshless discretization, with Xi nodes distributed within the body.

In general, this local domain is a circular or rectangular region, centered at the respective node, where the rigid-body displacement formulation of the work theorem is defined as a local form of mechanical equilibrium.

The local character of the MLS approximation is a consequence of the compact support of each node, where the respective MLS shape functions are defined. The size of the compact support, in turn, sets out, in a neighborhood of a sampling point, the respective domain of MLS approximation at this point. The domain of definition contains all the nodes whose MLS shape functions do not vanish at this sampling point. Therefore, the domain of influence of each node, is the union of the MLS domains of definition of all points in the local domain of the node.

Finally, local meshfree formulations use a node-by-node stiffness calculation to generate, in the domain of influence of the local node, the respective rows of the global stiffness matrix.

In the absence of body forces, the local form of the work theorem with the rigid-body displacement, Eq. (6), can be written simply as

$$\int_{\Gamma_Q - \Gamma_{Qt}} \mathbf{t}\, d\Gamma = -\int_{\Gamma_{Qt}} \bar{\mathbf{t}}\, d\Gamma \tag{9}$$

which represents mechanical equilibrium of boundary tractions of the local domain Ω_Q, associated with the field node $Q \in \Omega_Q$.

General numerical methods can be effectively formulated through a reduced integration of the equilibrium Eq. (9) which, in the simplest linear case, leads to a point-wise discrete, form that improves the accuracy and the computational efficiency, as numerical results clearly demonstrate.

Assuming a variation linear of the tractions along each boundary segment of the local domain, the local integral form of equilibrium can be evaluated with a single quadrature point, centered on each segment of the boundary. Applying this linear integration process in the Eq. (9), the following expression is obtained

$$\frac{L_i}{n_i}\sum_{l=1}^{n_i} t_{\mathrm{x}_l} = -\frac{L_t}{n_t}\sum_{j=1}^{n_t} \bar{\mathbf{t}}_{\mathrm{x}_j} \tag{10}$$

In which n_i and n_t denote the total number of the integration points, one per segment, defined on the interior local boundary $\Gamma_{Qi} = \Gamma_Q - \Gamma_{Qt} - \Gamma_{Qu}$, with length L_i, and the local static boundary Γ_{Qt}, with length L_t. This integrated equation represents a point-wise discrete form of the mechanical equilibrium of boundary tractions, evaluated at a set of points on the boundary of the local domain Ω_Q, as showed in the Fig. 4.

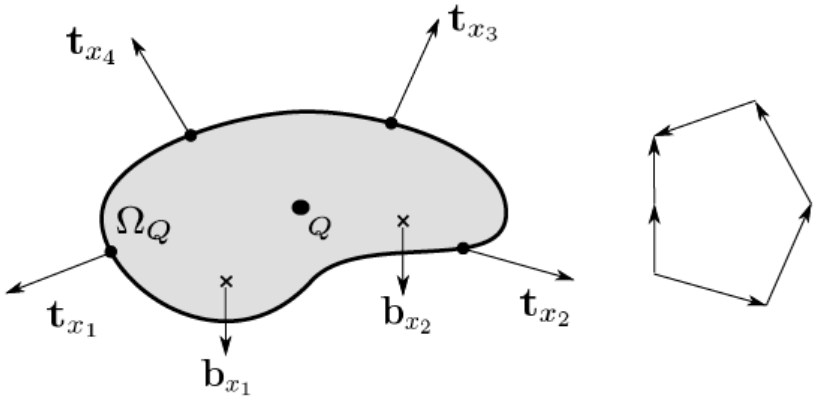

Figure 4. Schematic representation of the equilibrium of tractions and body forces, pointwisely defined at collocation points of a local domain associated with a field node *Q*.

Consider a meshfree discretization of the body. The local meshless method with reduce integration is used to compute the respective system of algebraic equations, in node by node process, throughout traction evaluation at each central point of the boundary segments of the integrated local form assigned to each node with rectangular local domain. Figure 5 represents these local domains with four boundary segments and one point on each segment.

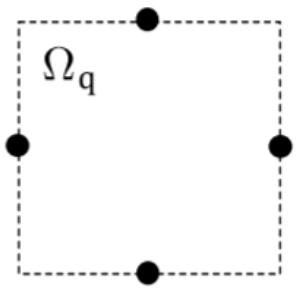

Figure 5. Schematic representation of rectangular local domain with one point on each side.

Discretization of Eq. (10) is carried out with the MLS approximation, for the local domain Ω_Q, in terms of the nodal unknowns $\hat{\mathbf{u}}$, thus leading to the system of two linear algebraic equations

$$\frac{L_i}{n_i}\sum_{l=1}^{n_i}\mathbf{n}_{x_l}\mathbf{DB}_{x_l}\hat{\mathbf{u}} = -\frac{L_t}{n_t}\sum_{j=1}^{n_t}\bar{\mathbf{t}}_{x_j} \tag{11}$$

that can be written as

$$\mathbf{K}_Q\hat{\mathbf{u}} = \mathbf{F}_Q \tag{12}$$

in which K_Q, the nodal stiffness matrix associated with the local Ω_Q, is a *2x2n* matrix given by

$$\mathbf{K}_Q = \frac{L_i}{n_i}\sum_{l=1}^{n_i}\mathbf{n}_{x_l}\mathbf{DB}_{x_l} \tag{13}$$

and $\mathbf{F}_Q$ is the respective force vector given by

$$\mathbf{F}_Q = -\frac{L_t}{n_t}\sum_{j=1}^{n_t}\bar{\mathbf{t}}_{x_j}. \tag{14}$$

Consider that the problem has a total of *N* field nodes *Q,* each one associated with the respective local region Ω_Q. Assembling Eq. (15), for all *M* interior and static – boundary field nodes leads to the global system of *2M x 2N* equations

$$\mathbf{K}\hat{\mathbf{u}} = \mathbf{F}. \tag{15}$$

Finally, the remaining equations are obtained from the *N – M* boundary field nodes on the kinematic boundary. For a field node on the kinematic boundary, a direct interpolation method is used to impose the Kinematic boundary condition as

$$u_k(x_j) = \sum_{i=1}^{n}\phi_i(x_j)\hat{u}_{ik} = \bar{\mathbf{u}}_k, \tag{16}$$

Or, in matrix form as

$$\mathbf{u}_k = \Phi_k\hat{u} = \bar{\mathbf{u}}_k, \tag{17}$$

with k = 1, 2, where $\bar{\mathbf{u}}_k$ is specified nodal displacement component. Equations (17) are directly assembled into the global system of equations (15).

It can be easily anticipated high computational efficiency, with very accurate results, of this local formulation with linear reduced integration. As a matter of fact, the nodal stiffness matrix is effectively computed, in Eq. (13), with only 4 integration points (1 integration point on each side of the local boundary), which basically implies a very short processing time to run the analysis. In addition, the reduced integration leads to high accuracy of the results, which plays a key role in the behavior of IMFM, since it implies a reduction of the nodal stiffness which, in turn, leads to an increase of the solution accuracy and, which is most important, presents no instabilities. For more information about the formulation for these method, see [14].

Parameters of the Meshfree Discretization

This section presents some numerical results for Cantilever beam and the Plate with a circular hole for different nodal configurations. The effects of the size of local support and quadrature domain are analyzed and compared with exact solution.

For a generic node i, the size of the local support Ω_S and the local domain of integration Ω_q are respectively given by

$$r\Omega_S = \alpha_S d_i, \tag{18}$$

$$r\Omega_q = \alpha_q d_i, \tag{19}$$

in which d_i represents the distance of the node i, to the nearest neighboring node; for the analysis is performed for two different values of the local support domain size ($\alpha_s = 2.00$ and $\alpha_s = 2.11$), and the local quadrature domain size (α_q) which vary 0.45 to 0.55 with increments 0.01.

Irregular nodal arrangement

The nodal irregularity is generated by changing randomly the coordinates of the nodal regularity distribution by small distance, this movement can be calculated by

$$x_{1i}' = x_{1i} \pm c_n d_{x_{1i}}, \tag{20}$$

$$x_{2i}' = x_i \pm c_n d_{x_{2i}}, \tag{21}$$

in which C_n is a parameter that controls the nodal irregularity and vary randomly in the range of 0.0 and 0.4. For nodes located in the boundary there are restrictions that depend on the position of the node.

Numerical Examples

Displacement and energy norms can be used for error estimation and can be computed, respectively as

$$\|u\| = \left[\int_\Omega u^T u d\Omega\right]^{1/2} \tag{22}$$

$$\|\varepsilon\| = \left[\frac{1}{2}\int_\Omega \varepsilon^T D\varepsilon d\Omega\right]^{1/2} \tag{23}$$

The relative error for $\|u\|$ and $\|\varepsilon\|$ is given, respectively by

$$r_u = \frac{\|u_{num} - u_{exact}\|}{\|u_{exact}\|} \tag{24}$$

$$r_\varepsilon = \frac{\|\varepsilon_{num} - \varepsilon_{exact}\|}{\|\varepsilon_{exact}\|} \tag{25}$$

Cantilever Beam

A Cantilever beam showed in Fig. 6, is subjected to a parabolic traction at the free end. The main properties are tabulated in Table 1 and the problem is solved for plane stress case.

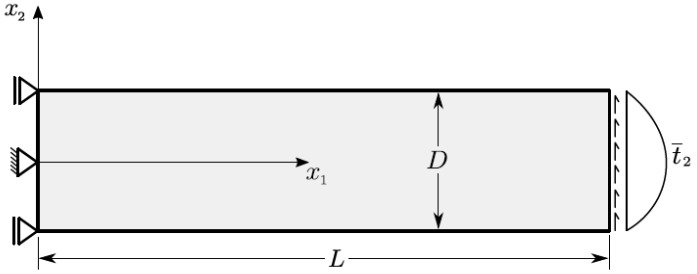

Figure 6. Cantilever beam

Table 1. Properties of Cantilever Beam

Parameters	Values
Height, D	12 m
Length, L	48 m
Thickness, t	1 m
Load, P	1000 N
Modulus of Elasticity, E	30 MPa
Poisson`s Ratio, ν	0.3

The parabolic traction and the moment of inertia is given by

$$\bar{t}_2(x_2) = -\frac{P}{2I}\left(\frac{D^2}{4} - x_2^2\right), \tag{26}$$

$$I = \frac{D^3}{12} \tag{27}$$

The exact solution of the problem is given by [19]. The equations for the exact displacement are:

$$u_1(x_1, x_2) = -\frac{Px_2}{6EI}\left[(6L - 3x_1) + (2+\nu)\left(x_2^2 - \frac{D^2}{4}\right)\right] \tag{28}$$

$$u_2(x_1, x_2) = \frac{P}{6EI}\left[3\nu x_2^2(L - x_1) + (4+5\nu)\frac{D^2 x_1}{4} + (3L - x_1)x_1^2\right] \tag{29}$$

And the exact stress components are given by

$$\sigma_{11}(x_1, x_2) = -\frac{P(L - x_1)x_2}{I} \tag{30}$$

$$\sigma_{12}(x_1, x_2) = -\frac{P}{2I}\left(\frac{D^2}{4} - x_2^{\,2}\right) \tag{31}$$

$$\sigma_{22}(x_1, x_2) = 0 \tag{32}$$

The IMFM is used for solving this problem, both a regular (c_n = 0.0) and irregular (c_n = 0.1, 0.2, 0.3 and 0.4) nodal distribution are employed with a discretization of 21 x 9 = 189 nodes.

In the first discretization the nodes located in the boundary have a regular distribution and nodes located inside of the beam have an irregular distribution; it is called Configuration A as is showed in Fig. 7 (presented by [20]) and Fig. 8.

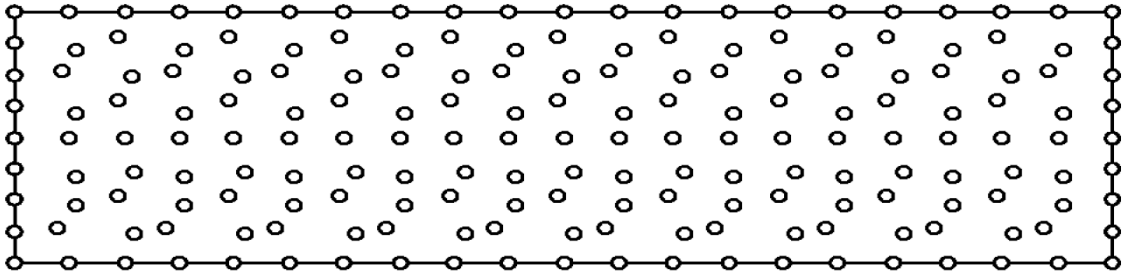

Figure 7. Irregular internal nodal arrangement for the Cantilever beam (MLPG [20]) – Configuration A

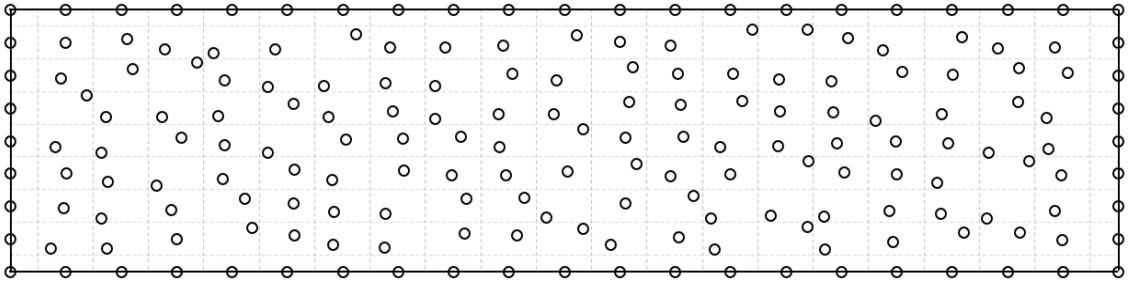

Figure 8. Irregular internal nodal arrangement for the Cantilever beam (IMFM) – Configuration A

Second discretization shows all nodes with an irregular distribution called Configuration B as is showed in Fig 9.

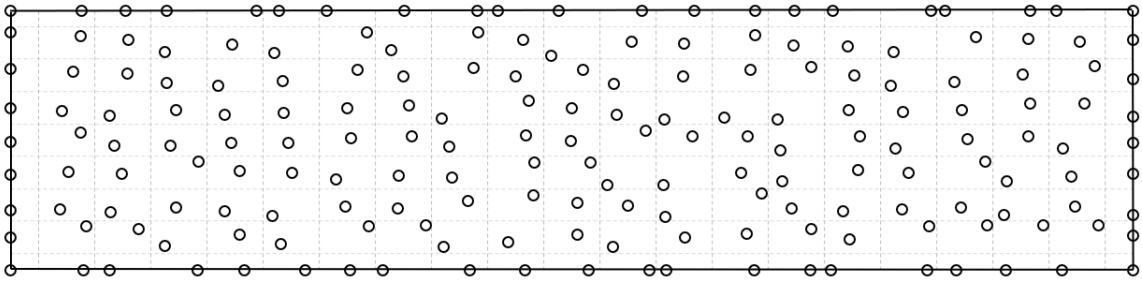

Figure 9. Irregular nodal arrangement for the Cantilever beam (IMFM) – Configuration B

Influence of the local support domain size (α_s)

This parameter must be greater than 1.0, the algorithm of MLS approximation may be singular and the shape function cannot be constructed for the small values. Initially, the influence of α_s in the solution is obtained for the local quadrature domain fixed ($\alpha_q = 0.5$), this value presented an optimal result for regular nodal distribution by [14].

Figure 10 shows the variation of relative error as a function of the size of the parameter of nodal irregularity which vary between 0.0 to 0.4 with 0.1 increments. Results are presented for two values of local support domain (α_s = 2.00 and α_s = 2.11) using both nodal configuration (A and B).

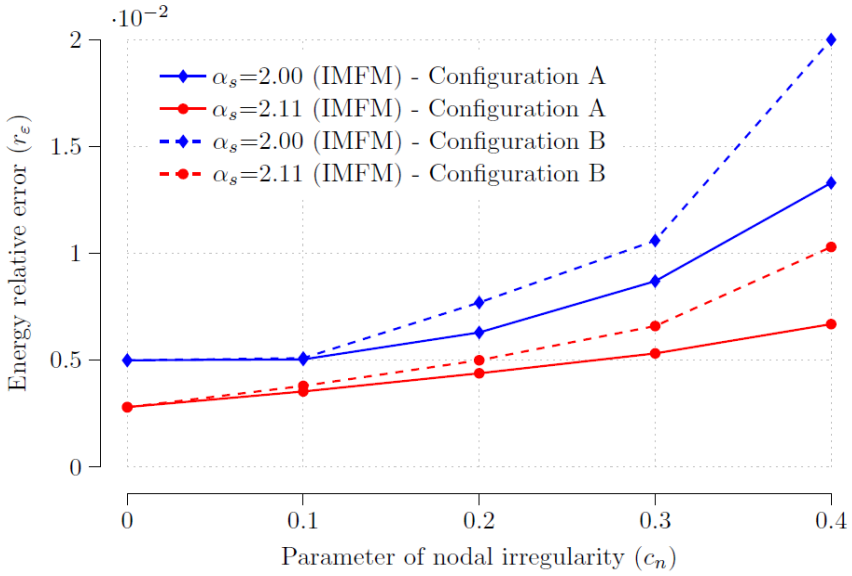

Figure 10. Effect of irregularity on the nodal arrangement on energy relative error with α_q = 0.5, carried out with 21 x 9 = 189 nodes.

Figure 10 shows that the value of 2.11 for the local support domain (α_s) presents low relative energy errors for model performed with both configurations. Additionally, the magnitude of the energy relative error increase with the nodal irregularity, presenting a directly proportional behavior between the two variables.

The energy relative error for two different methods is presented in Fig. 11, the same irregular nodal discretization called Configuration A is showed in the Fig. 7 for MLPG and the Fig. 8 for IMFM. The energy relative error for MLPG and IMFM have the same expression presented in Eq. 26 and 28. These values for MLPG were obtained in [20].

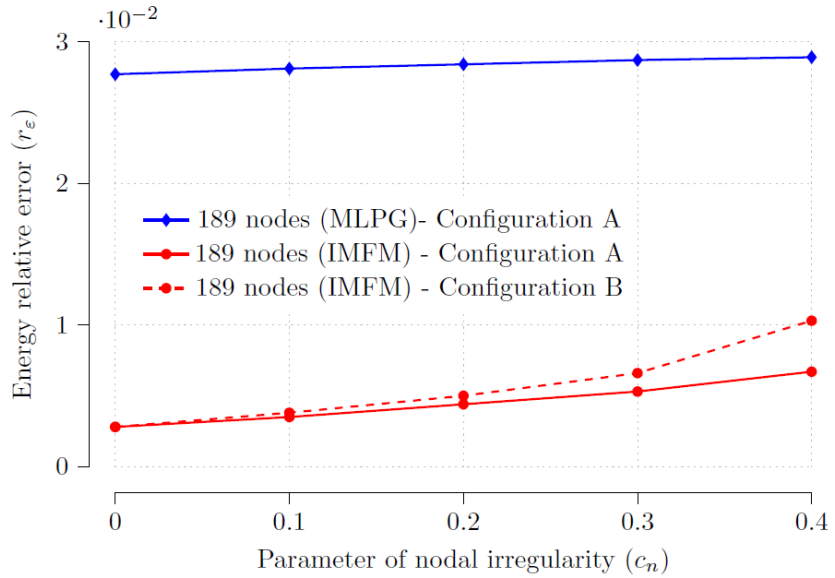

Figure 11. Effect of irregularity on the nodal arrangement on energy relative error for MLPG and IMFM, carried out with 21 x 9 = 189 nodes.

For the irregular nodal discretization IMFM and MLPG presented similar behavior for the configuration A, the IMFM presented more accuracy.

Influence of the local quadrature domain size (α_q)

This parameter must be less than 1.0, the reason is to ensure that the local sub – domains of the internal nodes are entirely within the solution domain, without being intersected by the global boundary. The influence of α_q is obtained for the local support domain fixed (α_s = 2.11).

Figure 12 shows the variation of relative error as a function of the size of the local support domain which vary between 0.45 to 0.55 with 0.01 increments. Results are presented for four values of parameter of nodal irregularity which vary between 0.0 to 0.4 with 0.1 increments; using the nodal configuration A.

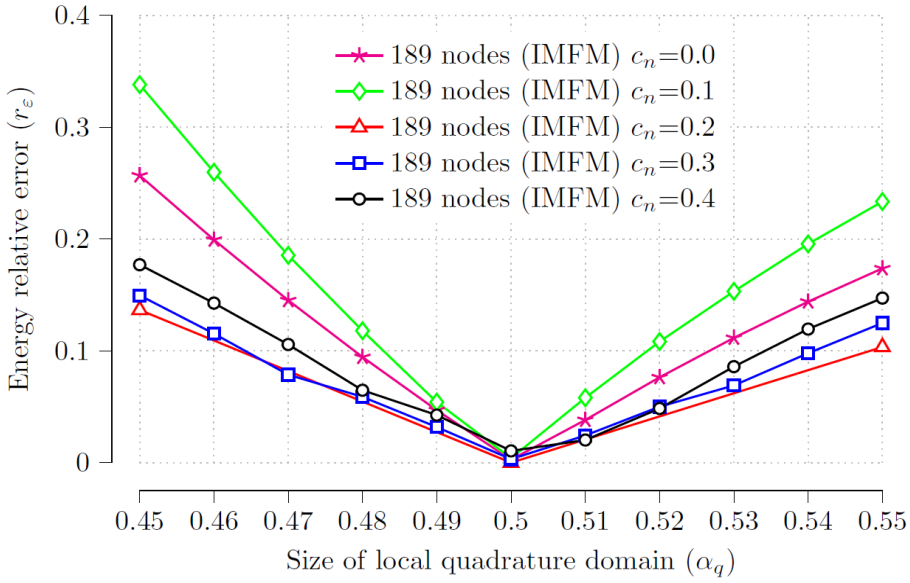

Figure 12. Effect of irregularity on the nodal arrangement on energy relative error with α_s = 2.11, carried out with 21 x 9 = 189 nodes.

Figure 12 shows that the value of 0.5 for the local quadrature domain (α_q) presents low relative energy errors for all values of parameter of nodal irregularity. Similar results are obtained for displacement relative error.

Influence nodal discretization

Other different irregular nodal discretization was carried out to know the influence on the accuracy on the energy and displacement relative error. Two additional configurations were presented with 11 x 5 = 55 nodes and 33 x 17 = 561 nodes.

Figure 13 and 14 show respectively, the variation of energy and displacement relative error as a function of the size of the parameter of nodal irregularity which vary between 0.0 to 0.4 with 0.1 increments. Results are presented for three nodal discretization using values fixed of the local support domain (α_s = 2.11) and the local quadrature domain (α_q = 0.5), using both nodal configuration (A and B).

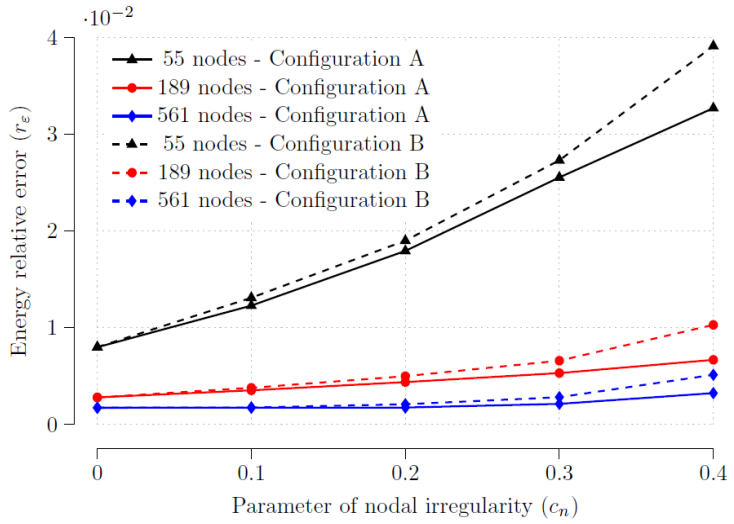

Figure 13. Effect of irregularity on the nodal arrangement on energy relative error with $\alpha_s = 2.11$ and $\alpha_q = 0.5$, carried out with 11 x 5 = 55 nodes, 21 x 9 = 189 nodes and 33 x 17 = 561 nodes.

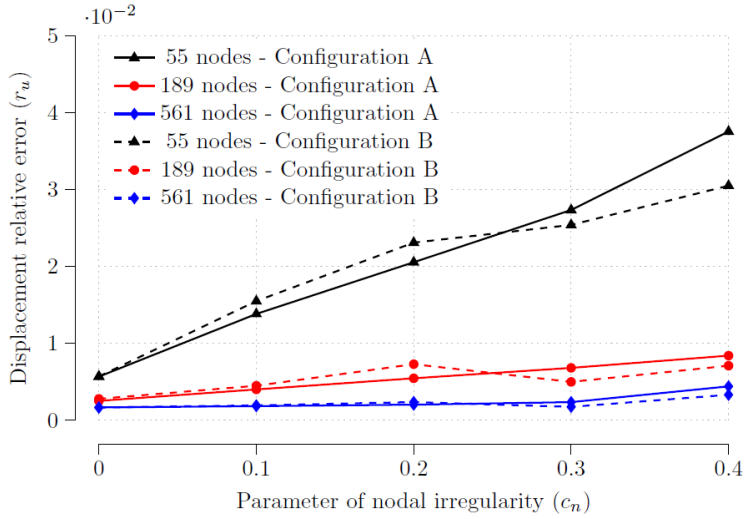

Figure 14. Effect of irregularity on the nodal arrangement on displacement relative error with $\alpha_s = 2.11$ and $\alpha_q = 0.5$, carried out with 11 x 5 = 55 nodes, 21 x 9 = 189 nodes and 33 x 17 = 561 nodes.

The Figure 13 and 14 shows that the energy and displacement relative error decreases with finer nodal distributions for both configuration. This result evidences that the meshless methods with reduce integration has the potential to be a very method including nodal arrangement with greater irregularity.

Conclusions

The effect of the nodal irregularity is very little on energy and displacement relative errors for different configuration and discretization. This fact reveals that the meshless methods with reduce integration (IMFM) and meshless Local Petrov Galerkin (MLPG) are stable for irregular nodal arrangements, but the IMFM presented more accuracy.

The nodal irregularity and the energy relative error presented a directly proportional relation for the cantilever beam. A similar behavior is showed for different mesh discretization, using a fixed value $\alpha_q = 0.5$ on the local quadrature domain.

The local quadrature domain ($\alpha_q = 0.5$) for regular and irregular nodal arrangement, different mesh discretization and any value of the local support domain presented the most accurate results for the cantilever beam.

The discretization with the nodes located in the boundary have a regular distribution and nodes located inside of the beam have an irregular distribution presents lower energy and displacement relative error that the discretization which all nodes have an irregular distribution.

Acknowledgments

The program PECC – *Pós-Graduação em Estruturas e Construção Civil*, Department of Civil and Environmental Engineering, Faculty of Technology, University of Brasília and CNPq – *Brazilian National Counsel of Technological and Scientific Development* for his PhD scholarship.

References

[1] Daxini, S. D. and Prajapati, J. M. (2014). A review on recent contribution of the meshfree methods to structure and fracture mechanics applications, *the scientific word journal* **2014**, 13 pages.

[2] Finalyson, B. A. (1972). The Method of Weighted Residuals and Vibrational Principles. Academic Press.

[3] Chen, J. S., Hillman, M. and Chi, S. W. (2017) Meshfree Methods: Progress made after 20 years, *Journal of Engineering Mechanics* **143**, 4.

[4] Nayroles, B., Touzot, G. and Villon, P. (1992). Generalized the Finite Element Method: Diffuse Approximation and Diffuse Elements, *Computational Mechanics* **10**, 307–318.

[5] Li, W. K., Jun, S., and Zhang, Y.F. (2007). Reproducing Kernel Particle Methods, *International Journal for Numerical methods in Engineering* **20**, 1081–1106.

[6] Belytshko, T., Lu, Y. Y. and Gu, L. (1994). Element – free Galerkin methods, *International Journal for Numerical Methods in Engineering* **37(2)**, 229–256.

[7] Atluri, S. N. and Zhu, T. (1998). A new Meshless Local Petrov-Galerkin (MLPG) approach in computational mechanics, *Computational Mechanics* **22(2)**, 117–127.

[8] Atluri, S. N. and Shen, S. (2002) The Meshless Local Petrov – Galerkin (MLPG) Method: A simple and Less-costly Alternative to the Finite Element and Boundary Element Methods, *CMES: Computer Modeling in Engineering and Sciences* **3(1)**, 11-51.

[9] Zhu, T., Zhang, J. and Atluri, S. N. (1998). A Local Boundary Integral Equation (LBIE) Method in Computational Mechanics and a Meshless Discretization Approach, *Computational Mechanics* 2**1**, 223–235.

[10] Liu, G. R. and Gu, Y. T. (2001). A Local Point Interpolation Method for Stress Analysis of Two-Dimensional Solids, *Structural Engineering and Mechanics* **11(2)**, 221–236.

[11] Liu, G. R., Yan, L., Wang, J. G. and Gu, Y. T. (2002). Point Interpolation Method Based on Local Residual Formulation Using Radial Basis Functions, *Structural Engineering and Mechanics* **14**, 713–732.

[12] Atluri, S. N. and Han, Z. D. and Rajendran, A. M. (2004). A New Implementation of the Meshless Finite Volume Method Through the MLPG Mixed Approach, *CMES: Computer Modeling in Engineering and Sciences* **6**, 491-513.

[13] Oliveira, T. and Portela, A. (2016). Weak – Form Collocation – a Local Meshless Method in Linear Elasticity. *Engineering Analysis with Boundary Elements* **73**, 144 – 160.

[14] Santana, E., Oliveira, T., Vélez, W. and Portela, A. (2017). Meshfree Method with Reduced Integration and Automatic Parameter Optimization, Computers and Structures (submitted).

[15] Fredholm, I. (1906) Solution d'un probléme fondamental de la théorie de l'éasticité. *Arkiv for Matematik Astronomi och Fysk 2* **28(1)**,1-8

[16] Fichera, G. (2006). Linear Elliptic Diferencial Systems and Eigenvalue Problems. Springer.
[17] Brebbia C. A. and Tottenham, H. (1985). Variational Basis of Aproximate Models in Continuum Mechanics. Southampton and Springer Verlag.
[18] Atluri, S. N. and Zhu, T. (2000). New Concepts in Meshless Methods, *International Journal for Numerical Methods in Engineering* **6**, 537-556.
[19] Timoshenko, S. P. and Goodier, J. N. (1970). *Theory of Elasticity*, 3rd edn, McGraw-Hill, New York, USA.
[20] Liu, G. R. (2003) Meshfree methods moving beyond the finite element method. CRC Press, 1st edition.